

Supporting Information

Sb-Enhanced Cs₃Cu₂I₅ Scintillators for Ionizing Radiation Detection

Yuwei Li¹, Haitao Tang¹, Bin Yu¹, Zhu Wang^{2,*}, Gaokui He^{3,*}, Qianqian Lin^{1,*}

¹ Key Lab of Artificial Micro- and Nano-Structures of Ministry of Education of China, Hubei LuoJia Laboratory, School of Physics and Technology, Wuhan University, Wuhan 430072, P. R. China

² Hubei Key Laboratory of Radiation Chemistry and Functional Materials, School of Nuclear Technology and Chemistry & Biology, Hubei University of Science and Technology, Xianning 437100, People's Republic of China

³ Department of Nuclear Technology and Application, China Institute of Atomic Energy, Beijing 102413, China.

Corresponding Author :

*E-mail: q.lin@whu.edu.cn; wangz428@outlook.com; 729785953@qq.com

1. Experimental Section

Chemicals and Materials: Cuprous iodide (CuI, 99.5%, Aladdin), Cesium iodide (CsI, 99.9%, Sigma-Aldrich), Triphenyl Antimony ($C_{18}H_{15}Sb$, Aladdin), N,N-Dimethylformamide (DMF, 99.9%, Aladdin), polymethyl methacrylate (PMMA, Shanghai Yuanye Bio-Technology Co., Ltd).

Preparation of $Cs_3Cu_2I_5:Sb@PMMA$ Composite Precursor Solution: Dissolve 0.6 mmol CsI, 0.4 mmol CuI in a chemical ratio in N, N-dimethylformamide (DMF) solvent to obtain a uniform precursor solution. Then, mix the doped triphenyl antimony in different proportions into the precursor solution, stir and mix evenly. Subsequently, 0.4 g PMMA was added to the precursor solution and stirred for 10 hours to obtain a homogeneous $Cs_3Cu_2I_5:Sb@PMMA$ composite precursor solution.

Preparation of $Cs_3Cu_2I_5:Sb@PMMA$ scintillators: The precursor solution was coated on a cleaned glass substrate. Slowly rotate until a uniform precursor film was obtained. Finally, the scintillator film was subjected to step-by-step annealing at 50°C, 10 minutes and 80°C, 5 minutes.

Characterizations: The crystal structure of the perovskite nanocrystals and powders were tested with X-ray diffraction (XRD), recorded using a Bruker Advance D8 X-ray diffractometer with Cu $K\alpha$ radiation at 1.5418 Å, scanned from 10° to 50°. Steady-state photoluminescence spectra were excited by a 405 nm CW laser, recorded by a fiber optic spectrometer (Ideaoptics, NOVA-EX). The absorption spectra were measured with a spectrometer (ThetaMetrisis, FR-Basic-UV/NIR-HR) via reflectance corrected transmittance mode. The commercially available SPELLMAN XRB011 tube (tungsten anode, 20 W maximum power output) was used as X-ray source. The radiation dose rate was calibrated with a standard dosimeter (Suhe Instrument Technology Co. LTD, XH-3525). The photocurrent of the scintillator covered silicon photodiode at different X-ray doses was recorded with a semiconductor Analyzer B1500A. A lead-containing, X-ray protective glass slide (1.5 cm) was placed between the detector and the scintillator to eliminate the influence of X-ray irradiation on the detector.

MTF measurements: We put the scintillator in front of the CCD camera, use the copper plate with different shapes to block the X-ray, and then directly take pictures and images. At the same time, the resolution is tested with copper plates with different line-pair widths, and the MTF is calculated by using the contrast of light and dark at the edges. The size of the pixel of camera chip used in this measurement is $9 \mu\text{m} \times 9 \mu\text{m}$. The resolution of copper plate is from 2 pairs to 16 pairs, and the thickness of copper plate is 0.15 mm.

light yield (LY) calculation: The relative light yield is calculated with the radioluminescence spectra. During testing, reference and target sample are placed in an integrated sphere. A commercial GAGG:Ce³⁺ single crystal was used as a benchmark. According to the proportion between the test signal and the LY, the LY values of the samples are obtained given by,

$$\frac{LY_{\text{sample}}}{LY_{\text{GAGG:Ce}^{3+}}} = \frac{S_{\text{sample}}}{S_{\text{GAGG:Ce}^{3+}}} \times \frac{\int I_{\text{sample}}(\lambda)S(\lambda)d\lambda / \int I_{\text{sample}}(\lambda)d\lambda}{\int I_{\text{GAGG:Ce}^{3+}}(\lambda)S(\lambda)d\lambda / \int I_{\text{GAGG:Ce}^{3+}}(\lambda)d\lambda}, \quad (\text{S1})$$

where $I(\lambda)$ is the RL intensity, and $S(\lambda)$ is the detection efficiency of photodetector. S_{sample} and $S_{\text{GAGG:Ce}^{3+}}$ are the area exposed to the X-ray of Cs₃Cu₂I₅:2%Sb@PMMA and GAGG:Ce³⁺, respectively.

2. Supplementary Figures

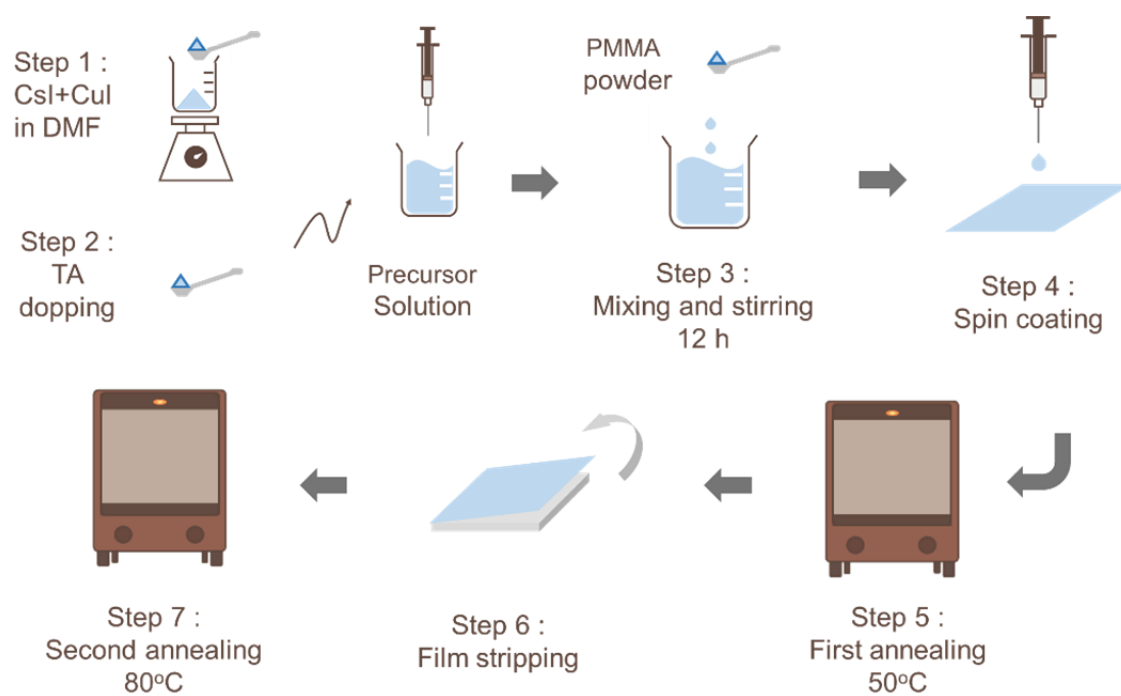


Figure S1. Schematic illustration of the preparation of Cs₃Cu₂I₅:Sb@PMMA scintillators.

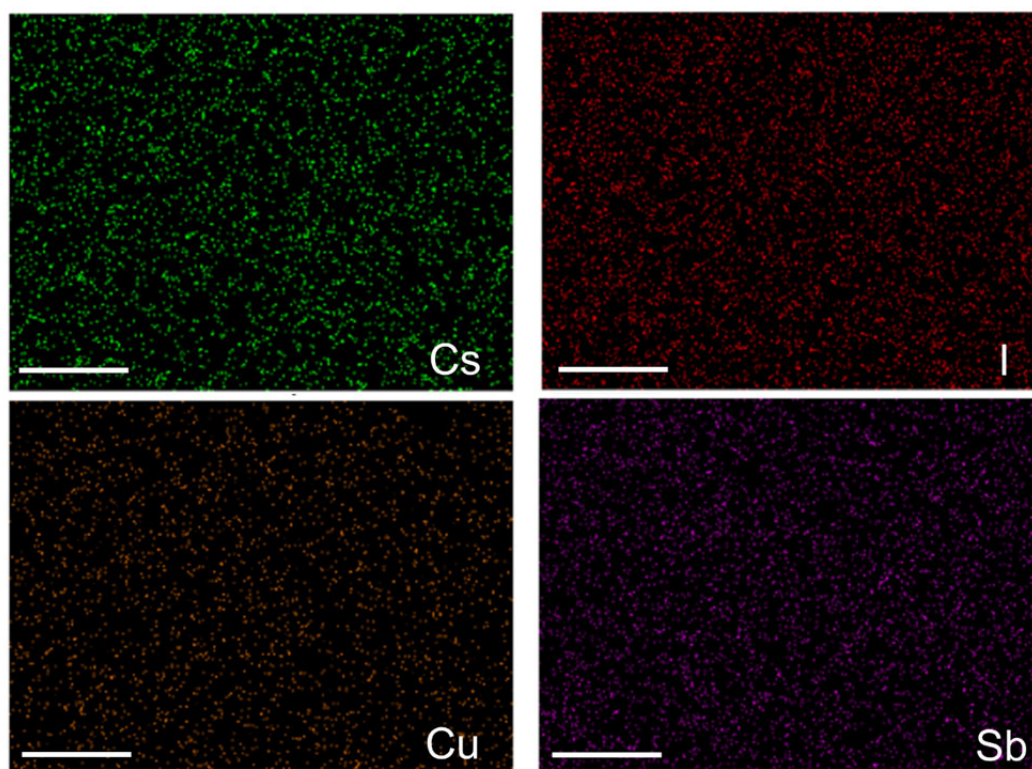


Figure S2. EDS mapping of Cs₃Cu₂I₅:Sb@PMMA. The scale bars are 25 μm.

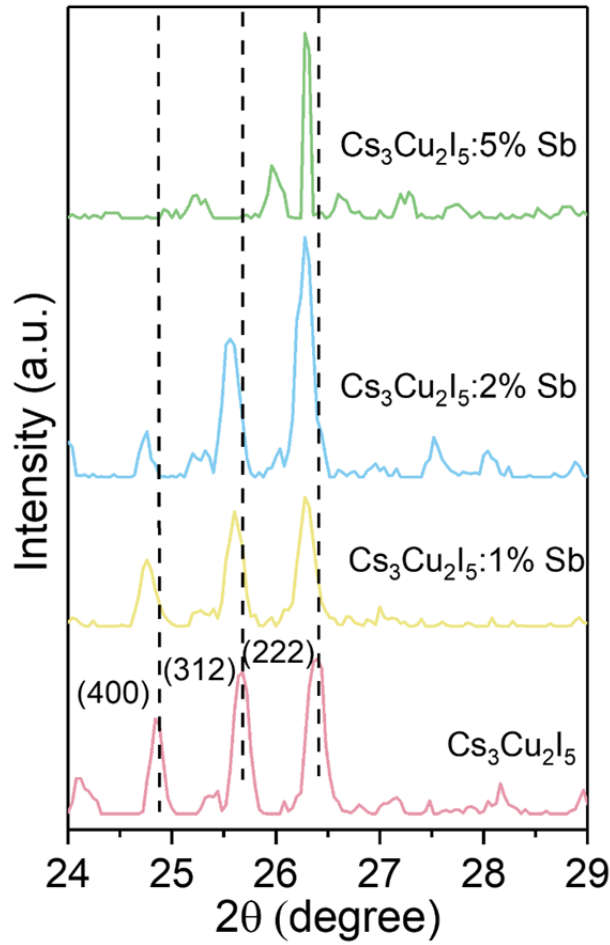


Figure S3. XRD fine scan of the Cs₃Cu₂I₅:Sb@PMMA samples with different doping concentrations.

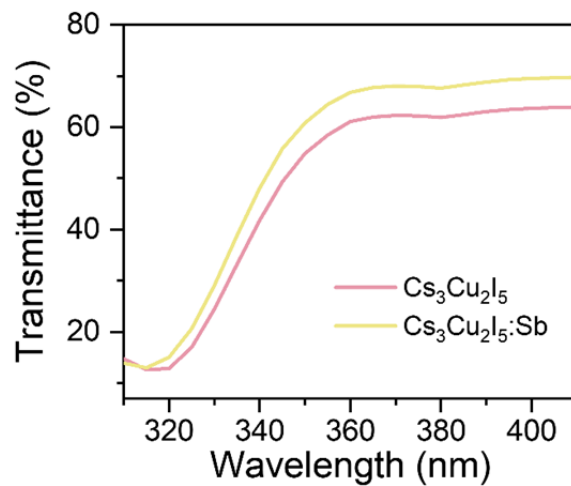


Figure S4. Comparison of the transmittance of the Cs₃Cu₂I₅@PMMA and Cs₃Cu₂I₅:Sb@PMMA scintillators.

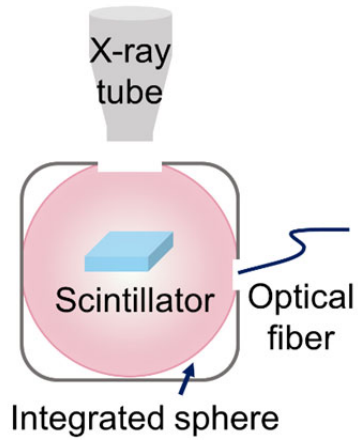


Figure S5. Schematic illustration of measuring the relative light yield.

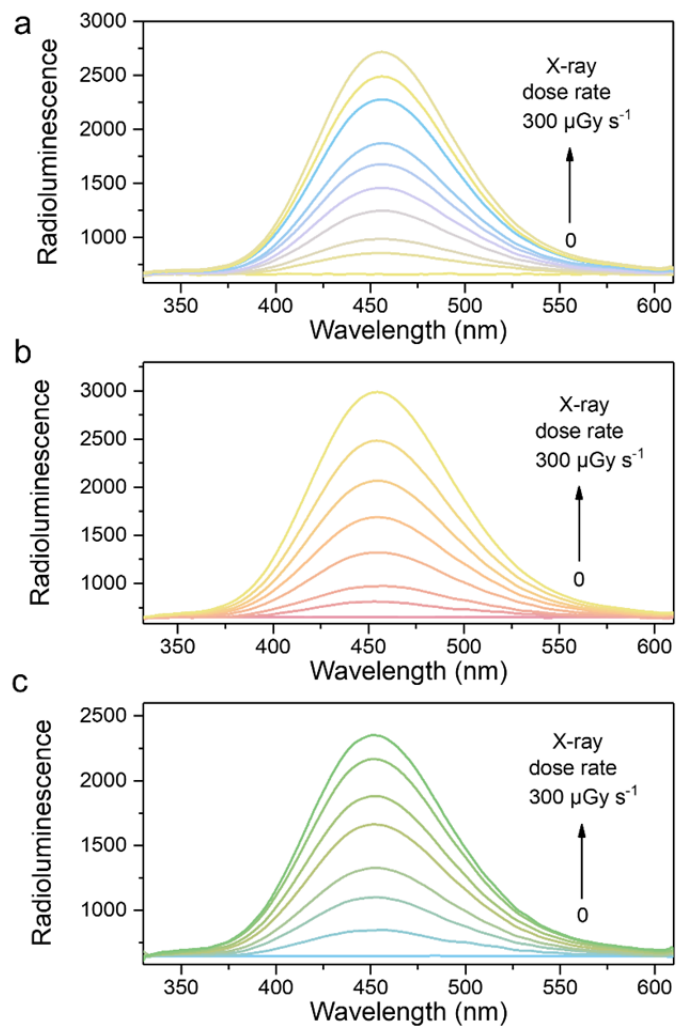


Figure S6. RL spectra of (a) $\text{Cs}_3\text{Cu}_2\text{I}_5@PMMA$, (b) $\text{Cs}_3\text{Cu}_2\text{I}_5:1\%\text{Sb}@PMMA$ and (c) $\text{Cs}_3\text{Cu}_2\text{I}_5:5\%\text{Sb}@PMMA$ scintillators with variable dose rates from 0 to $300 \mu\text{Gy s}^{-1}$.

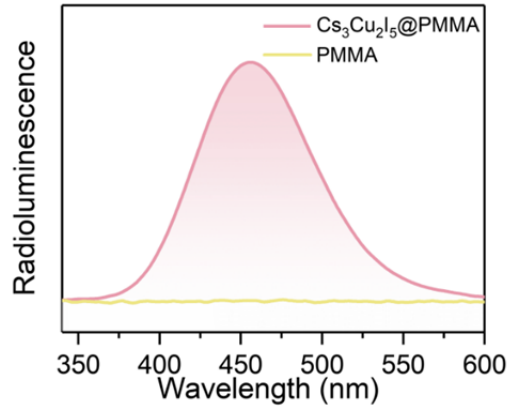


Figure S7. RL spectra of the $\text{Cs}_3\text{Cu}_2\text{I}_5@$ PMMA scintillator and PMMA.

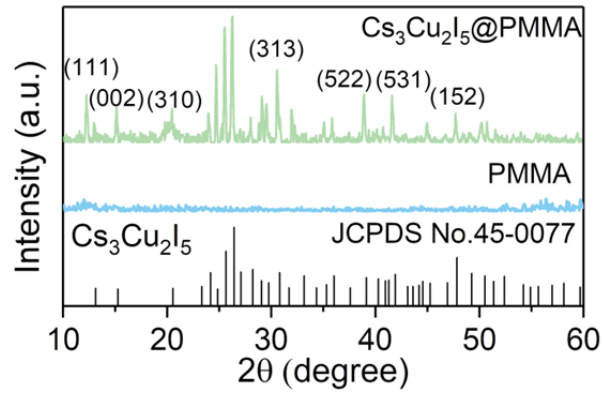


Figure S8. XRD patterns of the $\text{Cs}_3\text{Cu}_2\text{I}_5@$ PMMA scintillator and PMMA.

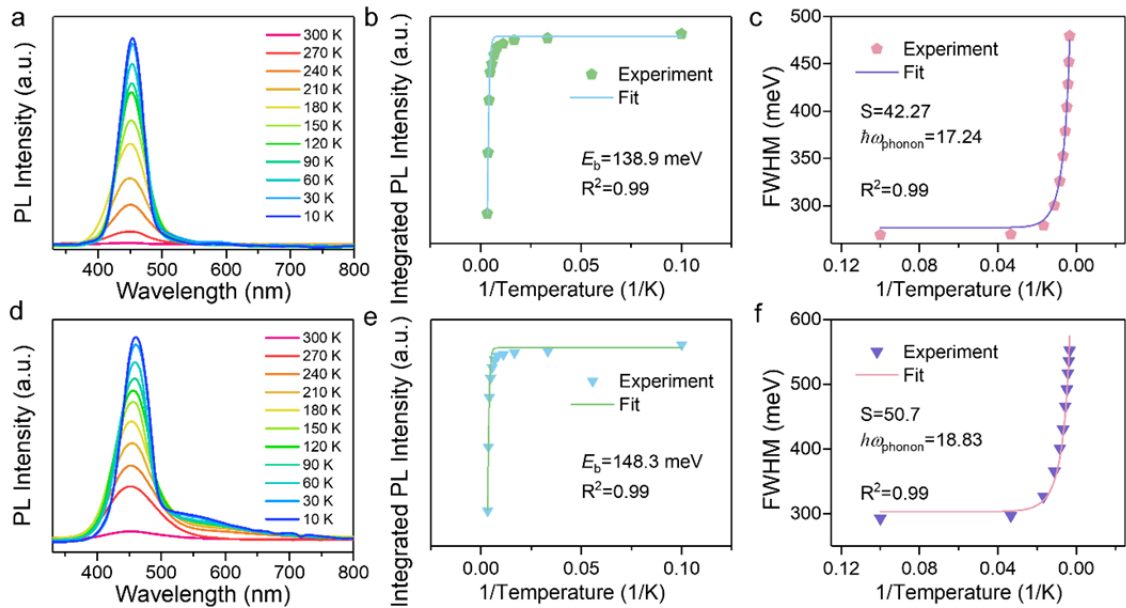


Figure S9. Temperature-dependent PL spectra (a) $\text{Cs}_3\text{Cu}_2\text{I}_5$ and (c) $\text{Cs}_3\text{Cu}_2\text{I}_5:2\%\text{Sb}$ ranging

from 10 to 300 K. Integrated PL intensity of (b) $\text{Cs}_3\text{Cu}_2\text{I}_5$ and (e) $\text{Cs}_3\text{Cu}_2\text{I}_5:2\%\text{Sb}$ versus $1/T$. FWHM of (c) $\text{Cs}_3\text{Cu}_2\text{I}_5$ and (f) $\text{Cs}_3\text{Cu}_2\text{I}_5:2\%\text{Sb}$ versus $1/T$.

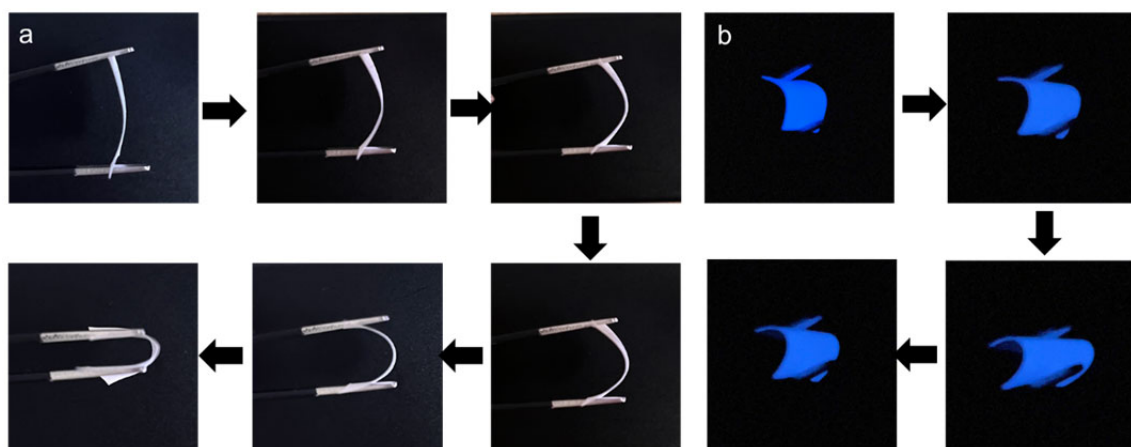


Figure S10. Flexibility test of the $\text{Cs}_3\text{Cu}_2\text{I}_5:2\%\text{Sb}@PMMA$ scintillator with (a) visible and (b) UV illumination (254 nm).

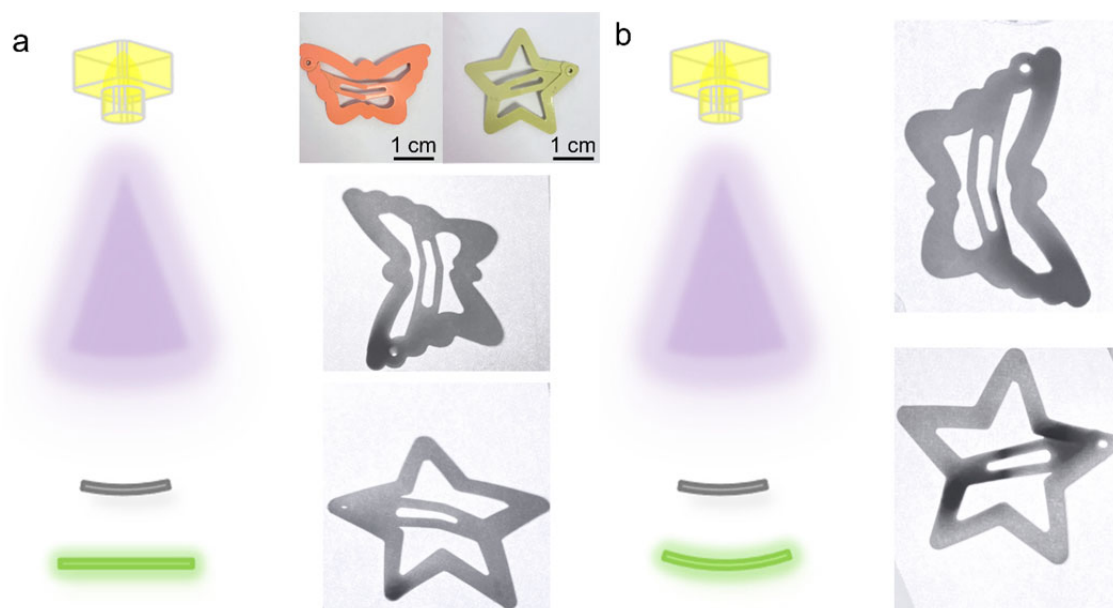


Figure S11. (a) Schematic diagram and (b) comparison of the X-ray imaging with a rigid scintillator (left) and flexible scintillator (right).

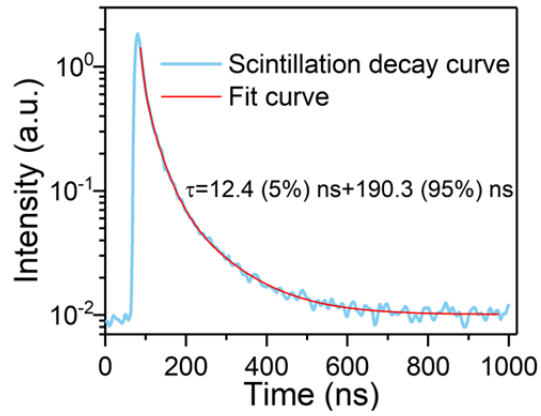


Figure S12. Stability test of scintillation decay time profile for $\text{Cs}_3\text{Cu}_2\text{I}_5:2\%\text{Sb}$, 30 days immersed in water.

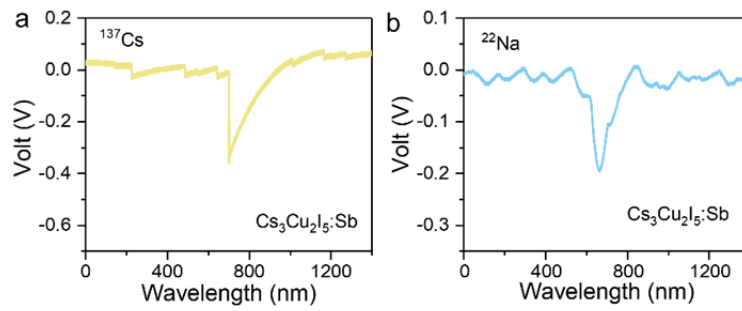


Figure S13. Responses of the optimized $\text{Cs}_3\text{Cu}_2\text{I}_5:\text{Sb}@\text{PMMA}$ scintillators to (a) ^{137}Cs and (b) ^{22}Na irradiation.